Homo-FRET Imaging Enables Quantification of Protein Cluster Sizes with Subcellular Resolution

Arjen N. Bader,[†] Erik G. Hofman,[‡] Jarno Voortman,[‡] Paul M. P. van Bergen en Henegouwen,[‡] and Hans C. Gerritsen[†*]
[†]Molecular Biophysics and [‡]Cellular Architecture and Dynamics, Universiteit Utrecht, Utrecht, The Netherlands

ABSTRACT   Fluorescence-anisotropy-based homo-FRET detection methods can be employed to study clustering of identical proteins in cells. Here, the potential of fluorescence anisotropy microscopy for the quantitative imaging of protein clusters with subcellular resolution is investigated. Steady-state and time-resolved anisotropy detection and both one- and two-photon excitation methods are compared. The methods are evaluated on cells expressing green fluorescent protein (GFP) constructs that contain one or two FK506-binding proteins. This makes it possible to control dimerization and oligomerization of the constructs and yields the experimental relation between anisotropy and cluster size. The results show that, independent of the experimental method, the commonly made assumption of complete depolarization after a single energy transfer step is not valid here. This is due to a nonrandom relative orientation of the fluorescent proteins. Our experiments show that this relative orientation is restricted by interactions between the GFP barrels. We describe how the experimental relation between anisotropy and cluster size can be employed in quantitative cluster size imaging experiments of other GFP fusions. Experiments on glycosylphosphatidylinisotol (GPI)-anchored proteins reveal that GPI forms clusters with an average size of more than two subunits. For epidermal growth factor receptor (EGFR), we observe that ~40% of the unstimulated receptors are present in the plasma membrane as preexisting dimers. Both examples reveal subcellular heterogeneities in cluster size and distribution.

INTRODUCTION

Binding events between proteins are essential in a broad range of cellular processes. In the field of signal transduction (1), for instance, transmission of the signal is governed by multiple interactions between proteins in the signal transduction chain. Initiation of the signaling cascade is usually mediated by the binding of identical proteins to each other, i.e., dimerization or oligomerization. Clustering of proteins is routinely investigated by coimmunoprecipitation or chemical cross-linking. Both of these techniques are prone to artifacts since the experimental conditions may induce clustering of proteins. More recently, microscopy methods based on fluorescence resonance energy transfer between identical fluorophores (homo-FRET) have been developed to study clustering processes (2–4). Similar to regular FRET, homo-FRET (5,6) involves the transfer of excited-state energy between fluorophores that are located within ~10 nm of each other. Because homo-FRET concerns energy transfer between identical fluorophores, it does not affect the emission spectrum or the fluorescence lifetime of the probes. In general, however, homo-FRET does result in a decrease of the fluorescence anisotropy of the probes. The combination of fluorescence anisotropy detection and microscopy affords the imaging of molecular-scale clustering of identical (bio)molecules in cells.

Various aspects of clustering can be studied using fluorescence anisotropy methods. For instance, from the time-resolved fluorescence anisotropy decay the rate of the homo transfer can be derived, which can be used to determine the distance between the fluorophores (3,6,7). In addition, it has been shown that fluorescence anisotropy can be used to determine the relative orientation of the fluorophores (7). Finally, the anisotropy can be related to the number of fluorophores per cluster (2–4,8). So far, cluster sizes of a few proteins have been determined by homo-FRET including human erythrocyte band 3, GPI-anchored proteins and the epidermal growth factor receptor (EGFR) (2–4,8).

To date, cluster sizes have been determined using (micro) spectroscopic approaches, where they are derived from a plot of the anisotropy versus the level of (controlled) photobleaching (3) or fractional labeling (4,9). This yields distributions of cluster sizes but no information about the spatial distribution of the clusters. In this work, we validate complementary approaches based on fluorescence anisotropy microscopy. The anisotropy in each pixel of the image is directly related to the cluster size. This approach makes it possible to quantify subcellular heterogeneities in protein clustering.

The theoretical framework that relates fluorescence anisotropy to cluster size has been provided by Runnels and Scarlata (10). Two critical factors are required for the determination of cluster size based on anisotropy data: the efficiency of the energy transfer and the anisotropy after energy transfer (2,10). Previously, we dealt with the former issue by utilizing time-gated fluorescence anisotropy imaging (2). The anisotropy after energy transfer, on the other hand, is difficult to predict. It depends on the relative orientation of the fluorophores. For organic dyes in solution, the relative orientation is random, but in complex biological samples, preferential orientations can be expected.

To circumvent these difficulties in applying the Runnels and Scarlata theory, we experimentally determine the relation between anisotropy and cluster size by controlled dimerization or oligomerization of green fluorescent protein (GFP) in cells. Regulation of dimerization or oligomerization was achieved by the fusion of monomeric GFP (mGFP) with the FK506-binding protein (FKBP12) that can be dimerized by binding of its ligand AP20187. Using this approach, we address the questions 1), what is the degree of depolarization due to homo-FRET in dimers and oligomers of GFP? 2), what are the advantages of utilizing time-resolved detection and/or two-photon excitation? 3), how is the observed depolarization related to the average number of fluorophores/ cluster? and 4), how can this be employed for direct quantitative imaging of protein cluster sizes?

We demonstrate (semi)quantitative cluster size imaging, including determination of the average number of fluorophores per cluster per pixel and monomer/oligomer fraction per pixel. Clustering was studied in two important model systems for cell signaling. First, lipid-mediated clustering of proteins in membrane domains (lipid rafts) was studied using glycosylphosphatidylinositol (GPI) linked to GFP. Second, preoligomerization of receptor tyrosine kinases was studied using the epidermal growth factor receptor (EGFR) C-terminally fused to mGFP. It is shown that both can form small nanoscale clusters in the plasma membrane of the resting cell. These examples demonstrate the potential of direct quantification of protein clustering by means of anisotropy-based homo-FRET imaging in (for example) cell signaling studies.

MATERIALS AND METHODS

Recombinant DNA constructs

Monomeric GFP was mutated at position 206 by site-directed mutagenesis on pEGFP-N3 (Clontech, Mountain View, CA) with the Quick-Change method using the primers forward 5′-cagtcc**aag**ctgagcaaagaccccaacgagaagcgcgat-cac-3′ and reverse 5′-gtgatcgcgcttctcgttggggtcttttgctcag**ctt**ggactg-3′ (with the mutagenic codon in bold print), in accordance with the methods of Zacharias et al. [11]. GFP and mGFP were amplified from pEGFP-N3 by polymerase chain reaction with flanking primers (forward 5′-atatactagtatggtgagca agggcgaggagctgttc-3′and reverse-5′ ttacttgtacagctcgtccatgccgagag-3′) using the high-fidelity DNA polymerase Phusion (Finnzymes, Espoo, Finland), and inserted into the SpeI and BamHI sites of the pC4-Fv1E vector (ARGENT Regulated Homodimerization Kit, Ariad Pharmaceuticals, Cambridge, MA) to produce pC4-Fv1-mGFP. pC4-Fv2-mGFP was constructed by exchanging the XbaI-SpeI fragment of pC4-Fv1-mGFP for an XbaI-SpeI fragment from pC4M-Fv2E (Ariad). Introduction of a flexible linker encoding four glycine and one serine residues (G4S), was performed by insertion of primers forward 5′-ctagtggtggcgggggatcca-3′ and reverse 5′-ctagtggatcccccgccacca-3′ at the SpeI site. All constructs were multiplied in Escherichia coli and isolated with an endotoxin-free plasmid isolation kit (Machery-Nagel, Dueren, Germany), and verified by DNA sequencing.

Cell culture and sample preparation

NIH 3T3 cells were cultured in Dulbecco's modified Eagle's medium (Invitrogen, Breda, The Netherlands) supplemented with 7.5% fetal bovine serum (v/v) and 2 mM L-glutamine at 37°C in the presence of 5% CO_2 under a humidified atmosphere. Before transfection, cells were trypsinized and seeded in six-well plates at 70% confluency. After 4 h, transfections were performed according to the manufacturer's protocol, using 4 μg of DNA and 10 μl of Lipofectamine 2000 (Invitrogen). Cells transfected with pC4-Fv-mGFP or pC4-Fv2-mGFP are called FKBP-mGFP or 2×FKBP-mGFP, respectively. At 12 h posttransfection, cells were trypsinized and allowed to grow on 18-mm coverslips (microscopy) or in 12-well plates (Blue-native PAGE). After 24 h, cells were either incubated for 1–2 h with 1 μM AP20187 (Ariad) or MOCK-treated (negative control) with 0.1% ethanol. For microscopy, cells grown to 20–30% confluency were washed with phosphate-buffered saline, fixed with freshly prepared 4% formaldehyde at 37°C for 20 min, and quenched by 100 mM glycine for 10 min. Coverslips were mounted with Mowiol and stored at −20°C until further use. It is important to note that these preparations are not expected to influence the clustering [12].

Blue-native gel electrophoresis

Cells expressing FKBP-GFP or 2×FKBP-GFP were grown to 80% confluency, either treated with AP20187 or Mock-treated as described, washed with phosphate-buffered saline, and lysed in 60 μl NativePAGE sample buffer (Invitrogen) supplemented with 1% n-dodecyl-β-D-maltoside and complete protease inhibitor cocktail (Roche, Indianapolis, IN). After centrifugation of the lysates for 30 min at 13,000 × g, 25 μl of the supernatant was taken and supplemented with NativePAGE G-250 sample additive (Invitrogen) to a final concentration of 0.25%. The lysates were loaded on a precast 3–12% NativePAGE gel (Invitrogen) and allowed to size-separate for 100 min at 150 V. Proteins were transferred to polyvinylidene fluoride (PVDF) membranes by semidry blotting, detected with a monoclonal anti-GFP IgG (Roche) in combination with donkey-antimouse IgG, and then visualized with an enhanced chemiluminescence reagent.

Fluorescence anisotropy imaging set-up

Fluorescence anisotropy imaging was carried out on a modified confocal scanning laser microscope (C1, Nikon Instruments Europe, Badhoevedorp, The Netherlands). For the one-photon excitation (OPE) experiments, excitation was provided by a 473-nm pulsed diode laser (BDL-473, Becker and Hickl, Berlin, Germany) operating at 50 MHz. For two-photon excitation (TPE) experiments, a Ti:Sapphire laser (Chameleon Ultra II, Coherent, Santa Clara, CA) running at 82 MHz and tuned to 860 nm was used. The excitation pulses were coupled directly into the modified C1 scan head. The excitation light is normally fiber-coupled into the scan head. This, however, would cause excessive broadening of the femtosecond laser pulse and complicate polarization-dependent measurements. Therefore, the fiber coupler and first lens in the excitation path of the scan head were removed, and the laser was directly coupled into the scan head. A linear polarizer (Meadowlark, Frederick, CO) was positioned in the laser beam to define the excitation polarization direction.

In the OPE experiments, a 60×, numerical aperture (NA) 1.20 water immersion objective (Plan Apo, Nikon) was used. The excitation beam did not fill the whole back aperture of the objective. The effective-excitation NA amounted to ~0.5. This NA did not affect the value of the initial anisotropy r_0 [13]; for GFP, an r_0 of 0.38 was found, which is similar to the value measured by Volkmer et al. [14]. As a consequence of the reduced-excitation NA, the resolution of the microscope is somewhat reduced.

In the TPE experiments, a 20×, NA 0.75 multiimmersion objective was used (Plan Fluor, Nikon, using water immersion). A beam expander was used to expand the diameter of the excitation beam and completely fill the back aperture of the objective. Again, the NA of the objective did not affect the observed r_0; for GFP, a value of $r_0 = 0.51$ was found, which is similar to the value measured by Volkmer et al. [14].

A broadband polarizing beam-splitter cube (OptoSigma, Santa Ana, CA) was used to split the emission into two channels, one parallel and one perpendicular with respect to the excitation light. The two emission channels were both fiber-coupled to detection systems consisting of a fluorescence

lifetime imaging module (LIMO (15), Nikon) (15) equipped with an internal photon-counting photomultiplier tube. For each pixel in the image, the LIMOs collect photons in four consecutive time gates each 2 ns wide. By employing two synchronized LIMOs, one for each polarization direction, a four-channel time-resolved anisotropy decay can be acquired for each pixel. An acquisition time of 3 ms/pixel was chosen and a threshold of 300 counts was applied. At this dwell time, the maximum number of counts/pixel amounted to ~4500. All images covered an area of 50 × 50 μm at 160 × 160 pixels.

Steady-state anisotropy images were obtained by summation of the intensities in all four gates. The procedures of data analysis, synchronization, and correction for sensitivity differences between the two channels were based on using reference dyes. This procedure has been described in detail previously (2,16).

THEORETICAL BACKGROUND

Steady-state fluorescence anisotropy

The relation between homo-FRET and fluorescence anisotropy has been extensively described in the literature (2,6,7,10). Briefly, the fluorescence anisotropy r is defined as the intensity-corrected difference between the emission parallel (I_{par}) and perpendicular (I_{per}) to the excitation polarization direction (5):

$$r(t) = \frac{I_{par} - I_{per}}{I_{par} + 2I_{per}}. \qquad (1)$$

In homo-FRET studies, fluorophores are used that exhibit minimal rotation during the fluorescence lifetime. After photoselection with polarized light, the donor fluorophores (D) exhibit a high anisotropy ($r_{mono} \approx 0.4$, where r_{mono} is defined as the average anisotropy of monomeric fluorophores in the absence of rotation). In contrast, after homo-FRET the fluorophores that act as acceptors (A) have a more random orientation and therefore lower anisotropy (r_{et} is here defined as the average anisotropy of fluorophores that are indirectly excited after homo-FRET). The measured anisotropy of clusters of fluorophores therefore contains contributions of both donor and acceptor fluorophores. Runnels and Scarlata (10) related the steady-state anisotropy (r_{ss}) to the cluster size (N, i.e., the average number of fluorophores/cluster), the relative orientation of the fluorophores (which determines the value of r_{et}), and homo-FRET efficiency, E. The latter is included as the product of the homo-FRET rate, ω, and fluorescence lifetime τ ($\omega\tau = E/(E - 1)$):

$$r_{ss} = r_{mono}\frac{1 + \omega\tau}{1 + N\omega\tau} + r_{et}\frac{(N - 1)\omega\tau}{1 + N\omega\tau}. \qquad (2)$$

Equation 2 is valid for measurements on a large number of fluorophore orientations to average out the orientation of individual fluorophores in a cluster. In fluorescence anisotropy imaging, typically hundreds of fluorophores are present in the detection volume, and the millisecond acquisition time introduces additional averaging due to (slow) rotations of the molecules. Both the homo-FRET rate, ω, and the anisotropy, r_{et}, need to be known to obtain quantitative information

about the cluster size, N. The rate, ω, can be derived from the time-resolved anisotropy decay. In steady-state fluorescence anisotropy imaging, however, ω is either estimated or assumed to be much faster than the rate of fluorescence. In the latter case, $\omega\tau$ approaches infinity, which effectively means that the homo-FRET efficiency is 1. Now, Eq. 2 simplifies to

$$r_{ss}(E = 1) = r_{mono}\frac{1}{N} + r_{et}\frac{N - 1}{N}. \qquad (3)$$

For randomly oriented fluorophores, the limiting anisotropy is ~0 ($r_{et} = 0.016$ (10,17)), but for nonrandom orientations, r_{et} will be higher. The value of r_{et} should therefore be experimentally determined.

Time-resolved fluorescence anisotropy

Time-resolved anisotropy decays provide more detailed information about homo-FRET than steady-state data. In the absence of rotation, the anisotropy decay due to homo-FRET can be written as (7,18)

$$r_{homo\text{-}FRET}(t) = (r_{mono} - r_{inf})e^{-2\omega t} + r_{inf}. \qquad (4)$$

Fitting the measured anisotropy decay using Eq. 4 yields the value of the homo-FRET rate. However, in imaging experiments, the number of photons that are typically collected per pixel is in practice not sufficient for a reasonable estimation of ω.

Within nanoseconds after the excitation pulse, the anisotropy levels off at the limiting anisotropy, r_{inf}. Homo-FRET has occurred multiple times and all fluorophores have equal probability of emitting a photon. This limiting anisotropy is identical to the steady-state anisotropy when fast and reversible homo-FRET takes place ($E = 1$, Eq. 3). As described in previous work (2), the limiting anisotropy is therefore a direct measure of the cluster size, N, independent of the efficiency of homo-FRET, and can be written as

$$r_{inf} = r_{ss}(E = 1) = r_{mono}\frac{1}{N} + r_{et}\frac{N - 1}{N}. \qquad (5)$$

The value of r_{inf} is always lower than or equal to the steady-state anisotropy, r_{ss}, and the reduction in r_{inf} due to clustering is often more pronounced than the reduction in r_{ss}. Consequently, variations in the degree of clustering can be more accurately determined by measuring r_{inf}. The extent of this improvement depends on the homo-FRET efficiency (2).

RESULTS

Controlled dimerization and oligomerization of GFP

To control dimerization and oligomerization of fluorescent protein, GFP was fused to one or two FK506-binding protein (FKBP) domains (19). Binding of one ligand (AP20187)

to two FKBP domains results in dimerization. Since AP20187 can easily pass the plasma membrane, dimerization of the GFP-FKBP fusion proteins can be induced by adding this ligand to cells expressing these constructs. Proteins that contain one FKBP domain will dimerize, whereas constructs that contain two FKBP domains will oligomerize in a broad distribution of cluster sizes. The constructs used here are composed of monomeric GFP (mGFP) directly attached to one or two FKBP domains. mGFP was made by mutating the alanine residue at position 206 into lysine. Here, we refer to the dimerizing and oligomerizing constructs as FKBP-mGFP and 2xFKBP-mGFP, respectively.

To validate the dimerization and oligomerization properties of the constructs, native polyacrylamide-gel electrophoresis (PAGE) of lysed NIH 3T3 cells was employed. Blue-native PAGE preserves the proteins in their native conformation (20). Here, cells were lysed in a buffer containing the comparatively mild detergent n-dodecyl-β-D-maltoside, which does not disturb the binding of ligand AP20187 to the FKBP domains. The lysate was size-separated on a native-PAGE gel, and after transfer of the proteins from the PAGE gel to a PVDF membrane, the mGFP tag was detected with a monoclonal antibody directed against GFP. In the absence of AP20187, FKBP-mGFP was found predominantly in the monomeric form (Fig. 1); only a small fraction of FKBP-mGFP was visible as dimers. Treatment of the cells with AP20187 resulted in the formation of mainly dimeric FKBP-mGFP. Also, the 2xFKBP-mGFP control, without AP20187, showed mainly monomers. Addition of AP20187 to the 2xFKBP-mGFP constructs resulted in a broad distribution of oligomers of the mGFP construct; the majority of the proteins appeared in dimeric, trimeric, or tetrameric form (Fig. 1).
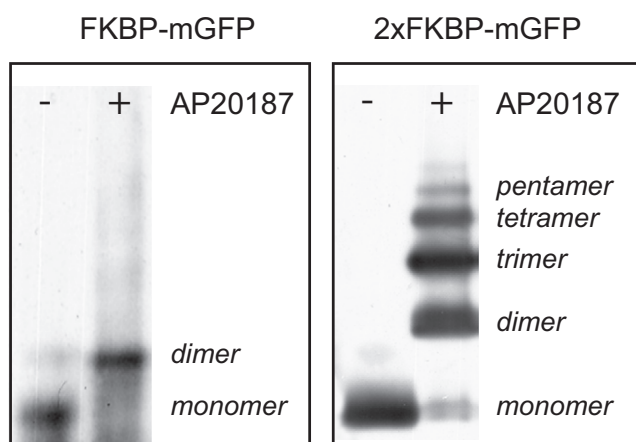

FIGURE 1 Native PAGE analysis of dimerization constructs. Cells expressing FKBP-mGFP or 2xFKBP-mGFP, either incubated with AP20187 or mock-treated, were lysed under nonreducing and nondenaturing conditions. After size separation on a NativePAGE gel and blotting to PVDF membrane, proteins were detected with anti-GFP antibodies.

Steady-state confocal fluorescence anisotropy

Steady-state fluorescence anisotropy images of NIH 3T3 cells transfected with the two FKBP-mGFP constructs were acquired using confocal fluorescence anisotropy imaging. The constructs were visible in both the cytoplasm and the nucleus of the cell (Fig. 2 A). For thresholded images, the intensities of all nonzero pixels were summed for both the parallel and perpendicular channels, and the average anisotropy values for five different cells were determined (Fig. 2 B). The initial anisotropy value (r_{mono}) for GFP in glycerol/buffer solution was found to be 0.382. Compared to this reference value, cytoplasmic FKBP-mGFP showed a small but significant drop in anisotropy of 0.019. For 2xFKBP-mGFP, the decrease in steady-state anisotropy amounted to 0.031. This decrease cannot be explained by an increase in rotational mobility of the fluorophore and is therefore attributed to homo-FRET. Apparently, even in the absence of dimerization-inducing ligand AP20187 some clustering occurs, which is in agreement with the PAGE experiments (Fig. 1). The fact that a lower anisotropy value was observed for the double FKBP construct than for single FKBP, suggests that the FKBP domain itself is (partly) responsible for this clustering. Incubation of the cells with 1 μM AP20187 for 2 h at 37°C resulted in a strong decrease of the steady-state anisotropy ($\Delta r = 0.055$, see Fig. 2 B). For the 2xFKBP-mGFP construct, an even larger decrease was observed ($\Delta r = 0.084$).

These data confirm that steady-state fluorescence anisotropy imaging can discriminate between monomers, dimers, and oligomers. However, despite the fact that the effect on the anisotropy of both dimerization and oligomerization is significant, the dynamic range of anisotropy reduction is limited.

Time-resolved confocal fluorescence anisotropy

Time-resolved detection of fluorescence anisotropy offers several advantages over steady-state methods. First, the decay due to rotation can be easily separated from that due to homo-FRET: homo-FRET results in a fast exponential decay of the anisotropy that levels off to a limiting anisotropy, r_{inf} (Fig. 3 A). The rate of anisotropy decay ($\sim 2\omega$) is in general much faster than the rotational correlation time of fluorophores such as GFP. Second, time-resolved detection affords a straightforward determination of r_{inf}. It can be directly obtained from the time-resolved anisotropy decay and provides a homo-FRET efficiency measure independent of the degree of clustering (Eq. 6). Time-resolved anisotropy imaging requires more complex experimental approaches than steady-state anisotropy imaging (2,16,21–24). Fortunately, comparatively low time resolution is sufficient to obtain information about the occurrence of homo-FRET. In this work, time-resolved anisotropy imaging was realized using time-gated detection with four 2-ns-wide gates. A schematic presentation of a typical homo-FRET decay, both at high time resolution and time-gated, is shown in Fig. 3 A.
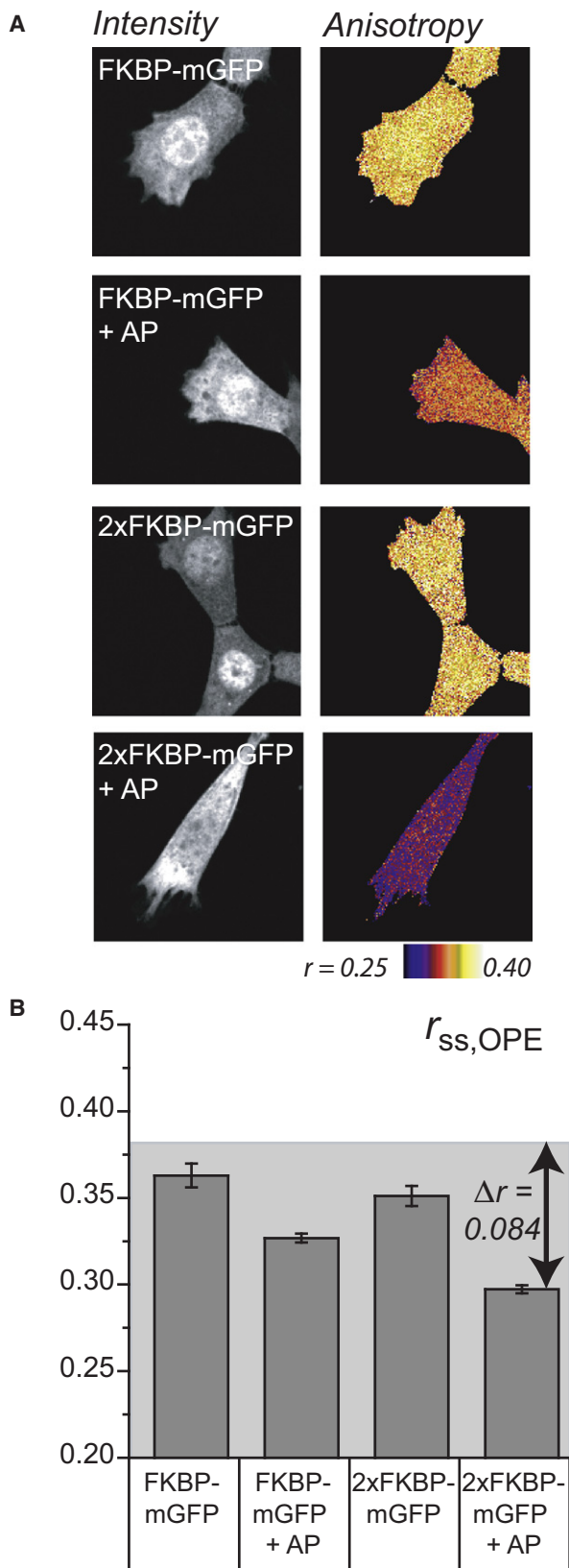
A

Intensity   Anisotropy

FKBP-mGFP

FKBP-mGFP + AP

2xFKBP-mGFP

2xFKBP-mGFP + AP

$r = 0.25$ 0.40

B

$r_{ss,OPE}$

$\Delta r = 0.084$

FKBP-mGFP   FKBP-mGFP + AP   2xFKBP-mGFP   2xFKBP-mGFP + AP

FIGURE 2 (*A*) Confocal steady-state intensity and fluorescence anisotropy images of cells expressing GFP-FKBP and GFP-2xFKBP, in both the presence and absence of AP20187 (*AP*). (*B*) Histograms of the average anisotropy of the samples in *A*. From each sample, five cells were imaged. The intensity values of all significant pixels were summed, and the overall anisotropy/cell was calculated. The error bars give the standard deviation between the cells. Here, $r_0 = 0.382$, as indicated by the top of the gray area in the histogram.

Time-gated anisotropy images were acquired for NIH 3T3 cells expressing the dimerization or oligomerization construct. The shape of the average time-gated anisotropy decay in the absence of the AP20187 ligand is typical for homo-FRET: after a fast initial drop the anisotropy remains approximately constant (Fig. 3 *B*). The images were further analyzed by calculating r_{inf} using Eq. 5. Already in the second gate the anisotropy approximates r_{inf}, which is consistent with the occurrence of homo-FRET with high energy transfer efficiency. Therefore, the intensities of the last three gates were summed for each pixel to improve statistics. The results of the time-gated anisotropy imaging experiments are summarized in Fig. 3 *C*. Here, average r_{inf} values over whole, thresholded images are shown for both the dimerization and oligomerization constructs. Similar to the steady-state results, a small depolarization was observed in the absence of AP20187. Addition of the clustering ligand induced a further decrease in anisotropy r_{inf} of $\Delta r = 0.070$ for the dimerization construct and $\Delta r = 0.106$ for the oligomerization construct. The main difference between steady-state and limiting anisotropy r_{inf} is that an increase in dynamic range is observed. For 2xFKBP-mGFP with AP20187, the dynamic range increases by ~25% compared to the steady-state results.

Two-photon excitation fluorescence anisotropy

Two-photon excitation experiments were carried out to explore the potential of the increased anisotropy range of this excitation method in homo-FRET studies (Fig. 4). An increase in anisotropy reduction due to homo-FRET is expected as the theoretical maximum value of r_0 for TPE increases to 0.57 (14,23). Two-photon excitation measurements of cells expressing either FKBP-mGFP or 2xFKBP-mGFP were performed employing both steady-state and time-resolved detection. The average anisotropy decays exhibited profiles similar to the one-photon excitation profiles. However, the value of r_{mono} increased from 0.38 for OPE to 0.51 for TPE. As a result of the increased anisotropy range, the depolarization due to dimerization increased to $\Delta r = 0.083$ and $\Delta r = 0.107$ for steady-state and time-resolved detection, respectively. For oligomerization (2xFKBP + AP20187) the depolarization increased to $\Delta r = 0.127$ and $\Delta r = 0.154$ for steady-state and time-resolved detection, respectively.

These results demonstrate that when TPE is used, depolarization due to homo-FRET is enlarged by 45–50% compared to that seen with OPE. Potentially, the increased depolarization range offers the possibility of improved contrast between different-sized clusters.
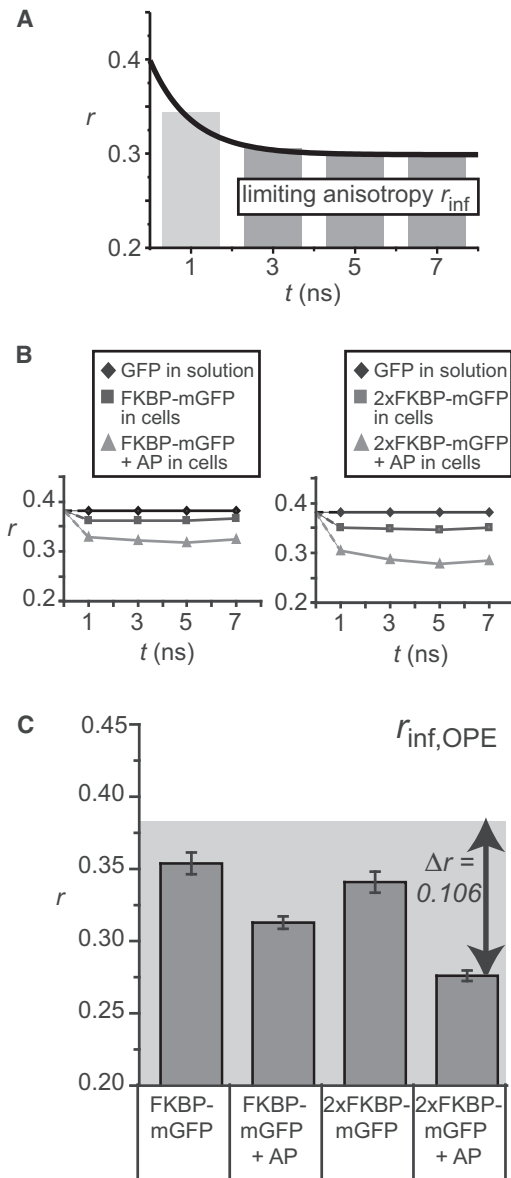
FIGURE 3 Confocal time-gated fluorescence anisotropy imaging. (*A*) A schematic representation of a typical *r* decay due to homo-FRET. The limiting anisotropy (r_{inf}) is independent of the homo-FRET efficiency for $E > 0.5$. (*B*) Time-resolved anisotropy decays of cells expressing FKBP-mGFP and 2xFKBP-mGFP, in both the presence and absence of AP20187 (*AP*). For all images in each sample, the intensities/gate in the significant pixels were summed to create the average *r* decays. (*C*) The average anisotropy for each sample is plotted in a histogram. The dynamic range (Δr) is larger than for r_{ss} (compare Fig. 2 *B*). Here, $r_0 = 0.382$, indicated by the top of the gray area in the histogram.

FIGURE 4 Two-photon excitation fluorescence anisotropy imaging. Similar to Figs. 2 *B* and 3 *C*, the average anisotropy/sample was measured using TPE. For both steady-state (*A*) and time-gated detection (*B*), the dynamic range (Δr) increases compared to that found using OPE. Here, $r_0 = 0.505$, indicated by the top of the gray area in the histogram.

Relating anisotropy to cluster size

When relating the anisotropy to cluster size, it is most convenient to use r_{inf}. For both OPE and TPE, dimerization resulted in a r_{inf} reduction of only ~20%, whereas for oligomerization, a reduction of ~30% was observed. This means that the commonly used simplification of Runnels and Scarlata theory ($r = r_{mono}/N$) is not valid for GFP probes. It demonstrates that
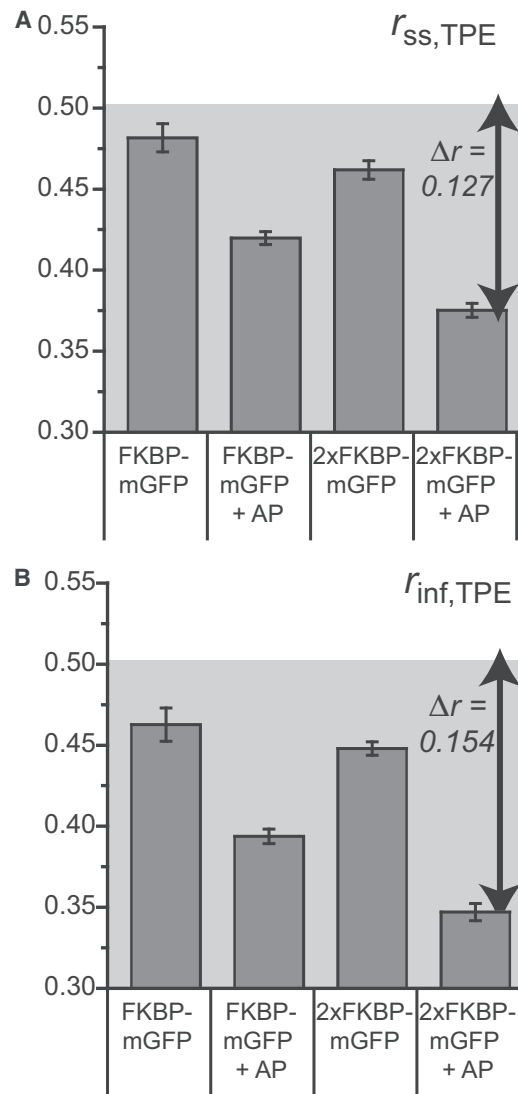
the anisotropy after energy transfer (r_{et}) is not negligible and the relative orientations of the fluorophores is nonrandom. This could be induced either by binding of the FKBP domains to AP20187, or by binding at (semi)specific dimerization sites on the fluorophores themselves. To reduce the former effect, an FKBP-mGFP construct was made with a flexible linker five amino acids long between FKBP and mGFP (FKBP-g4s-mGFP). The presence of this linker should reduce the effect of the FKBP domain on the orientation distribution of the GFP. However, the linker did not increase the reduction of r_{inf} (Fig. 5 *A*).

We therefore hypothesize that even for monomeric GFP, sites are present that allow binding between mGFPs. Such binding determines the relative orientation of the fluorophores. The observed efficiency of the transfer ($E \approx 0.7$)

corresponds to an interfluorophore distance of ~4 nm ($R_0 = 4.65$ nm (3)). This distance is comparable to the size of GFP: a barrel with diameter 2.5 nm and height 4 nm (25). Compared to these dimensions, the interfluorophore distance in dimerized FKBP-mGFP allows binding at low-affinity dimerization sites. To further investigate the role of dimerization sites the monomeric GFP (mGFP) was replaced by GFP. Although the latter contains a functional dimerization domain, this did not yield a difference in anisotropy (Fig. 5 A). This is consistent with crystal-structure data from GFP showing that GFP dimerization results in an antiparallel orientation of the two fluorescent proteins (25). Sterical effects are not likely to allow such dimerization when GFP is attached to dimerized FKBP, even in the presence of the flexible linker. Our results suggest (weak) binding between two parallel GFPs that is not related to the main dimerization site. Even when the strength of this interaction is weak, it is still likely to occur, since the local concentration of the fluorophores in clusters is high. A schematic representation of this model is depicted in Fig. 5 B.

An important consequence of this model is that the relative orientation of the fluorophores depends on the GFP probe, i.e., not on the fused protein. This means that the anisotropy of mGFP fused to FKBP can serve as a reference value for mGFP fused to other proteins. The main prerequisite is that there is a flexible linker between the protein and (m)GFP, so that the (m)GFPs can assume their "preferred" relative orientation. It is important to note that this aspect can be verified based on the FRET efficiency: when $E > 0.7$, the interfluorophore distance is <4 nm and the (m)GFP barrels interact with each other. If so, the relative depolarization is $r_{inf}/r_{mono} = 0.312/0.382 = 0.82$ for dimers and $r_{inf}/r_{mono} = 0.276/0.382 = 0.72$ for oligomers (see Fig. 3 C).

The signal level required to discriminate different cluster sizes is determined by photon statistics. The intensity dependence of the theoretical standard deviation in anisotropy is described by Lidke et al. (26). This work shows that under the current experimental conditions, at least 1200 counts are needed to discriminate $N_{av} = 1$, 2, and ≥ 3 (Fig. 6).

At such signal levels, anisotropy images can be converted to (semiquantitative) cluster size images. Fig. 6 shows that relative depolarization (r_{inf}/r_{mono}) values >0.91 correspond to $N_{av} = 1$, those in the range 0.91–0.77 correspond to $N_{av} = 2$, and those in the range 0.77–0 correspond to $N_{av} \geq 3$. The physical meaning of N_{av} is given by Runnels and Scarlata theory: $N_{av} = 1$ corresponds to all fluorophores being directly excited, $N_{av} = 2$ occurs when the number of donor fluorophores equals the number of acceptor fluorophores, and $N_{av} \geq 3$ occurs when there is an excess of acceptor fluorophores. On a pixel level, typically hundreds of fluorophores are present, and N_{av} is a measure of the average cluster size. Note, $N_{av} = 2$ does not necessarily mean that all molecules are present as dimers, but can also indicate a mixture of monomers and large-size clusters.

Two applications of FKBP-calibrated homo-FRET clustering are given in the next section. Although the FKBP
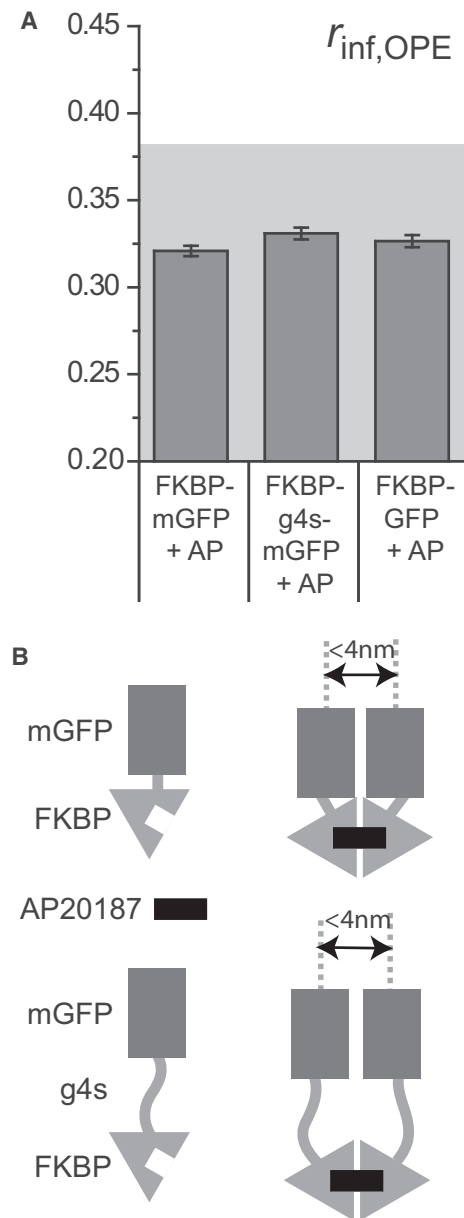

FIGURE 5 (A) Anisotropy reduction due to homo-FRET is not altered by the presence/absence of a flexible linker or dimerization domain in the fluorophore. (B) Schematic diagram of possible relative orientations of the GFP fluorophores in FKBP-induced dimers. Here, $r_0 = 0.382$, indicated by the top of the gray area in the histogram.

fusions are cytoplasmic, their anisotropies can be employed as references for membrane-bound proteins provided sufficient orientational averaging occurs. In our case, sufficient averaging is expected to occur due to the presence of the flexible GFP linker and membrane curvature.

Nanoscale clustering of GPI-GFP

Confocal time-resolved anisotropy imaging was used to determine the cluster size in resting cells of a GFP fused with a GPI-anchor, a model for GPI-anchored proteins (3).
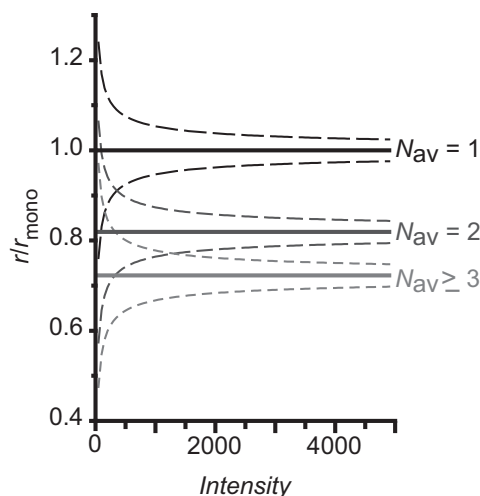
FIGURE 6 Significance of direct cluster size determination from anisotropy data. The solid curves represent the measured r_{inf}/r_{mono} of GFP in glycerol/buffer solution ($N_{av} = 1$), in cells expressing FKBP-mGFP in the presence of AP20187 ($N_{av} = 2$), or in cells expressing 2xFKBP-mGFP in the presence of AP20187 ($N_{av} \geq 3$). The dashed curves are the theoretical standard deviations plotted as a function of the intensity, as formulated by Lidke et al. (26). Note that the standard deviations are also dependent on the factor that corrects for differences in transmission between the parallel and perpendicular channels (the G-factor). Here, an average G-factor of 0.35 was used.
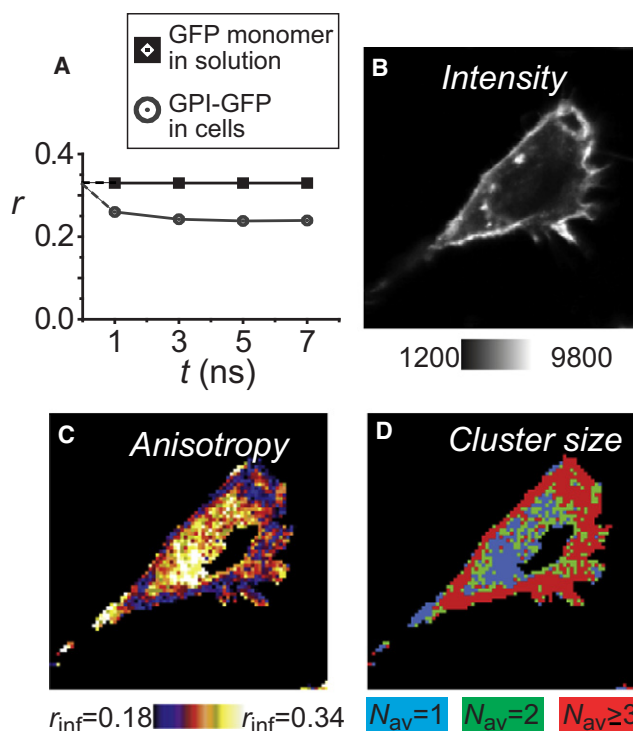

FIGURE 7 Confocal time-gated anisotropy imaging shows nanoscale clustering of GPI-GFP in the plasma membrane. (A) Time-resolved anisotropy decay, obtained by summing the intensities/gate in the significant pixels. (B–D) Intensity (B), limiting anisotropy (C), and cluster-size (D) images of cells expressing GPI-GFP. The latter two images are binned to 80×80 pixels. Threshold = 1200 counts, $r_{mono} = 0.330$.

The construct encoding for GPI-GFP was stably expressed in NIH 3T3 cells. Cells expressing this protein display GFP fluorescence at distinct locations in the cells, although the Golgi apparatus and plasma membrane are the most prominent sites (Fig. 7 B). Due to the absence of rotational effects, the average time-resolved anisotropy decay found in these cells can be attributed to homo-FRET (Fig. 7 A). The fast initial decay in anisotropy indicates a high energy transfer efficiency ($E > 0.7$), proving that the interfluorophore distance is small enough to allow interaction between the GFP barrels. The interactions of the GFPs in GPI-GFP are expected as to be similar to those in the FKBP constructs. Therefore, the r_{inf} image (Fig. 7 C) can be transferred to a cluster-size image (Fig. 7 D) using the experimental data on FKBP. As expected, the anisotropy and cluster size images demonstrate differential clustering behavior of GPI-GFP, dependent on the subcellular localization. The majority of GPI-GFP is located at the plasma membrane, where it forms small clusters. The size of these clusters is, on average, larger than dimers. In contrast, the Golgi-located GPI-GFP is predominantly present as monomers.

Nanoscale clustering of EGFR

In resting cells, a fraction of the EGFR in the plasma membrane is clustered. These clusters are composed of dimers and higher-order oligomers. If we assume that the anisotropy of these clusters resembles the reference anisotropy of oligomers ($r_{inf,clus} / r_{mono} = 0.72$, as derived from Fig. 3 C),

then the fraction of fluorophores in a cluster ($F_{cluster}$) can be estimated using

$$F_{cluster} = \frac{r_{mono} - r_{inf}}{r_{mono} - r_{inf,clus}}. \tag{6}$$

In the case of monomers, the measured anisotropy, r_{inf}, equals r_{mono}, and $F_{cluster}$ is zero. On the other hand, when r_{inf} is equal to the reference anisotropy of clusters, $r_{inf,cluster}$, then $F_{cluster} = 1$.

To determine $F_{cluster}$ of EGFR in resting cells, NIH 3T3 cells were stably transfected with a construct encoding the human EGFR fused with mGFP. Comparative flow cytometry indicates that the cell line expresses the EGFR-GFP fusion proteins at an average level of ~50,000 receptors/cell. Moreover, control experiments show that activation kinetics and activation levels of EGFR or EGFR-GFP are indistinguishable, which is in agreement with other studies (data not shown). To determine the degree of EGFR-mGFP clustering in nonstimulated cells, confocal time-resolved anisotropy images were recorded (Fig. 8). The time-resolved anisotropy decay of all the significant pixels in the cells shows that fast homo-FRET results in depolarization of the emission (Fig. 8 A). Averaged over five cells, a depolarization r_{inf}/r_{mono} of 0.89 was observed. According to Eq. 6, this corresponds to a cluster fraction of 0.4.
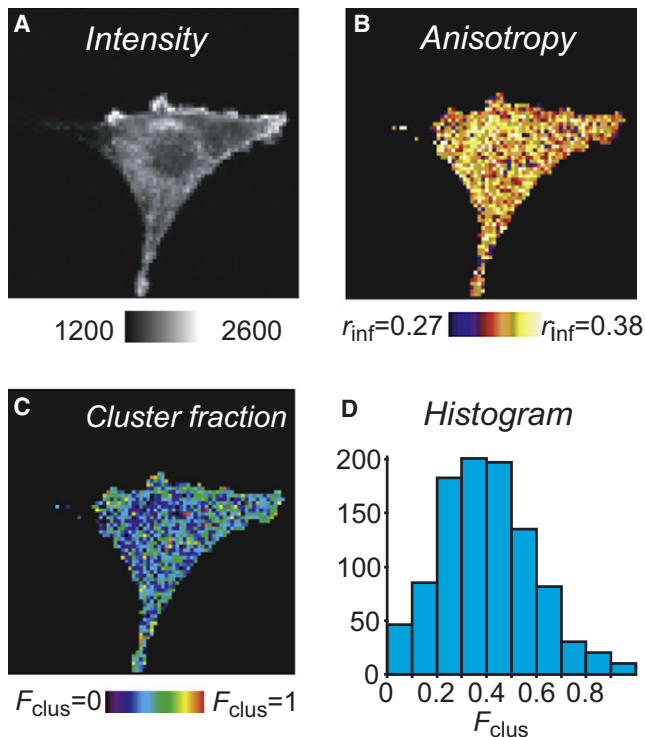
FIGURE 8 Confocal time-gated anisotropy imaging shows 40% clustering of EGFR-mGFP in the plasma membrane. (*A–C*) Intensity (*A*), limiting anisotropy (*B*), and fraction of clusters (*C*) in a cell expressing EGFR-mGFP. The images are binned to 80×80 pixels. Threshold = 1200 counts, $r_{mono} = 0.381$. (*D*) Histogram of $F_{cluster}$ for one image. The width of the histogram is predominantly determined by photon statistics (26).

DISCUSSION

In this work, we demonstrate that fluorescence anisotropy microscopy methods can be used to directly determine the degree of clustering of proteins with subcellular resolution. Quantification of cluster sizes is achieved by carrying out reference measurements during controlled dimerization and oligomerization of mGFP fused to (2x)FKBP. These measurements reveal a stepwise decrease in the anisotropy.

Time-resolved detection has distinct advantages over steady-state measurements; it can be used to verify that homo-FRET occurs and to determine r_{inf}. For TPE, the dynamic range is increased. However, it is also more prone to photobleaching; TPE photobleach rates are proportional to I^n, where I is the excitation power and $n > 2$ (27). Therefore, the count rates are comparatively low, which may compromise the accuracy of the anisotropy. The benefits of the improved dynamic range can thereby be lost.

An important observation here is that in GFP-labeled protein clusters the orientation of the fluorophores is not random. A model is proposed in which chemical interactions between (m)GFP barrels fix the orientation of the fluorophores. This orientation will affect both the efficiency of the transfer and depolarization of the emission after homo-FRET (r_{et}). When fluorophores in a cluster have similar orientation, homo-FRET will be efficient, but the effect of homo-FRET on the anisotropy will be minor. Conversely, for fluorophores with a more perpendicular orientation, E will be low, but the effect on the anisotropy large. The former is observed in this work as well as in other time-resolved homo-FRET studies that utilize GFP-tagged proteins (3,7). Typical measurements are $r_{inf}/r_{mono} = 0.7$–0.9 and $E > 0.5$.

These results indicate a complication of the use of GFP probes in homo-FRET studies. The commonly made assumption that $r_{et} = 0$ is not valid for (m)GFP, as is also expected to be true for analogs of GFP. Nevertheless, it is possible to correlate anisotropy and cluster size by using reference anisotropy values from constructs that enable controlled dimerization/oligomerization. At sufficiently high signals, this approach affords discrimination of monomers, dimers, and oligomers (Fig. 6). Distinguishing larger-scale organization will be difficult, even with the appropriate reference samples. In the case of nanoscale organization of a large number of proteins with diameter larger than that of GFP, multiple small subclusters of interacting GFP fluorophores are expected. In such a case, homo-FRET is more efficient between fluorophores in these subclusters, whereas homo-FRET between the subclusters is less likely. As a consequence, the actual size of the protein clusters is underestimated.

The methodology described here is complementary to the controlled photobleaching or fractional-labeling-based homo-FRET cluster size determination methods. An advantage of our method is that subcellular heterogeneities can be imaged. Another major advantage is that it can be used in live-cell imaging. Nevertheless, "indirect" methods are more accurate; various models of *N*-mer distributions can be incorporated in the analysis (2–4).

As an example of time-resolved anisotropy imaging, we studied the clustering of a model molecule for GPI-anchored proteins, GPI-GFP. Specifically in the plasma membrane, a large number of pixels was found with cluster size ≥ 3. The absence of GPI-GFP clusters in the Golgi system suggests the presence of a factor in the plasma membrane that stimulates cluster formation of GPI-GFP. This factor is apparently absent in the Golgi. As GPI-anchored proteins are found to partition into lipid rafts (3), the lipid composition might be responsible for the clustering process.

In addition to GPI-GFP we studied the cluster behavior of EGFR. The EGF receptor is the most studied member of the family of receptor protein tyrosine kinases. The classical model of EGFR activation predicts that EGF is inducing receptor dimerization followed by an allosteric activation of the EGFR tyrosine kinase. However, there is a growing body of evidence that the EGFR is already present on the plasma membrane as receptor preclusters before activation. For instance, the oligomeric state of the EGFR has been studied using electron microscopy, and it was demonstrated that 55% of gold-labeled EGFR is monomeric, 40% is

dimerized, and 5% is oligomerized (28). Using fluorescence correlation spectroscopy and fluorescent brightness analysis, Saffrian et al. found that 70% of the fluorescence comes from monomers, 20% from dimers, and 10% from oligomers (29). These results are in reasonable agreement with our finding that ~40% of the EGFR is in the predimerized or oligomerized state. It would be interesting to see the effect of EGF on this distribution, which will be the subject of future research.

An important question that remains is, which factors are regulating the predimer formation of the EGFR? Similar to the situation for GPI-GFP, predimer formation of EGFRs might be induced by their presence in lipid rafts. Recent findings suggest that receptor aggregation is sensitive to the lipid composition of the plasma membrane (30). Since predimers are more efficient in binding the ligand (31), this factor might regulate the sensitivity of the cell for EGFR signaling. The described methodology will be very powerful in further research on the role of protein clustering and lipid domains in cell signaling pathways.

REFERENCES

1. Krauss, G. 2001. Biochemistry of Signal Transduction and Regulation. Wiley-VCH, Weinheim, Germany.

2. Bader, A. N., E. G. Hofman, P. M. P. Van Bergen en Henegouwen, and H. C. Gerritsen. 2007. Imaging of protein cluster sizes by means of confocal time-gated fluorescence anisotropy microscopy. *Opt. Express.* 15:6934–6945.

3. Sharma, P., R. Varma, R. C. Sarasij, K. IraGousset, et al. 2004. Nanoscale organization of multiple GPI-anchored proteins in living cell membranes. *Cell.* 116:577–589.

4. Yeow, E. K. L., and A. H. A. Clayton. 2007. Enumeration of oligomerization states of membrane proteins in living cells by homo-FRET spectroscopy and microscopy: theory and application. *Biophys. J.* 92:3098–3104.

5. Valeur, B. 2002. Molecular Fluorescence. Principles and Applications. Wiley, Weinheim, Germany.

6. Jares-Erijman, E. A., and T. M. Jovin. 2003. FRET imaging. *Nat. Biotechnol.* 21:1387–1395.

7. Gautier, I., M. Tramier, C. Durieux, J. Coppey, R. B. Pansu, et al. 2001. Homo-FRET microscopy in living cells to measure monomer-dimer transition of GFP-tagged proteins. *Biophys. J.* 80:3000–3008.

8. Szabo, A., G. Horvath, J. Szollosi, and P. Nagy. 2008. Quantitative characterization of the large-scale association of ErbB1 and ErbB2 by flow cytometric homo-FRET measurements. *Biophys. J.* 95:2086–2096.

9. Blackman, S. M., D. W. Piston, and A. H. Beth. 1998. Oligomeric state of human erythrocyte band 3 measured by fluorescence resonance energy homotransfer. *Biophys. J.* 75:1117–1130.

10. Runnels, L. W., and S. F. Scarlata. 1995. Theory and application of fluorescence homotransfer to melittin oligomerization. *Biophys. J.* 69:1569–1583.

11. Zacharias, D. A., J. D. Violin, A. C. Newton, and R. Y. Tsien. 2002. Partitioning of lipid-modified monomeric GFPs into membrane microdomains of live cells. *Science.* 296:913–916.

12. Bancroft, J. D., and A. Stevens. 1982. Theory and Practice of Histological Techniques. Churchill Livingstone, New York.

13. Axelrod, D. 1989. Fluorescence polarization microscopy. *Methods Cell Biol.* 30:333–352.

14. Volkmer, A., V. Subramaniam, D. J. S. Birch, and T. M. Jovin. 2000. One- and two-photon excited fluorescence lifetimes and anisotropy decays of green fluorescent proteins. *Biophys. J.* 78:1589–1598.

15. de Grauw, C. J., and H. C. Gerritsen. 2001. Multiple time-gate module for fluorescence lifetime imaging. *Appl. Spectrosc.* 55:670–678.

16. Bader, A. N., E. G. Hofman, P. Van Bergen en Henegouwen, and H.C. Gerritsen. 2007. Confocal time-resolved fluorescence anisotropy imaging. *In* Progress in Biomedical Optics and Imaging. *Proc. SPIE.* 6441:0C.

17. Arganovich, V. M., and M. D. Galanin. 1982. Electronic excitation energy transfer in condensed matter. North-Holland Publishing, Amsterdam.

18. Tanaka, F., and N. Mataga. 1979. Theory of time-dependent photoselection in interacting fixed systems. *Photochem. Photobiol.* 29:1091–1097.

19. Fooksman, D. R., G. K. Gronvall, Q. Tang, and M. Edidin. 2006. Clustering class I MHC modulates sensitivity of T cell recognition. *J. Immunol.* 176:6673–6680.

20. Wittig, I., H.-P. Braun, and H. Schägger. 2006. Blue native PAGE. *Nat. Protoc.* 1:418–428.

21. Siegel, J., K. Suhling, S. Leveque-Fort, S. E. D. Webb, D. M. Davis, et al. 2003. Wide-field time-resolved fluorescence anisotropy imaging (TR-FAIM): imaging the rotational mobility of a fluorophore. *Rev. Sci. Instrum.* 74:182–192.

22. Clayton, A. H. A., Q. S. Hanley, D. J. Arndt-Jovin, V. Subramaniam, and T. M. Jovin. 2002. Dynamic fluorescence anisotropy imaging microscopy in the frequency domain (rFLIM). *Biophys. J.* 83:1631–1649.

23. Levitt, J. A., N. Sergent, A. Chauveau, M. K. Kuimova, P. R. Barber, et al. 2008. Multidimensional multiphoton fluorescence lifetime imaging of cells. *In* Progress in Biomedical Optics and Imaging. *Proc. SPIE.* 6860:1G.

24. Buehler, C., C. Y. Dong, P. T. C. So, T. French, and E. Gratton. 2000. Time-resolved polarization imaging by pump-probe (stimulated emission) fluorescence microscopy. *Biophys. J.* 79:536–549.

25. Yang, F., L. G. Moss, and G. N. Phillips, Jr. 1996. The molecular structure of green fluorescent protein. *Nat. Biotechnol.* 14:1246–1251.

26. Lidke, K. A., B. Rieger, D. S. Lidke, and T. M. Jovin. 2005. The role of photon statistics in fluorescence anisotropy imaging. *IEEE Trans. Image Process.* 14:1237–1245.

27. Patterson, G. H., and D. W. Piston. 2000. Photobleaching in two-photon excitation microscopy. *Biophys. J.* 78:2159–2162.

28. Van Belzen, N., P. J. Rijken, W. J. Hage, S. W. De Laat, A. J. Verkleij, et al. 1988. Direct visualization and quantitative analysis of epidermal growth factor-induced receptor clustering. *J. Cell. Physiol.* 134: 413–420.

29. Saffarian, S., Y. Li, E. L. Elson, and L. J. Pike. 2007. Oligomerization of the EGF receptor investigated by live cell fluorescence intensity distribution analysis. *Biophys. J.* 93:1021–1031.

30. Hofman, E. G., M. O. Ruonala, A. N. Bader, D. van den Heuvel, J. Voortman, R. C. Roovers, A. J. Verkleij, H. C. Gerritsen, and P. M. P. van Bergen en Henegouwen. 2008. EGF induces coalescence of different lipid rafts. *J. Cell Sci.* 121:2519–2528.

31. Teramura, Y., J. Ichinose, H. Takagi, K. Nishida, T. Yanagida, et al. 2006. Single-molecule analysis of epidermal growth factor binding on the surface of living cells. *EMBO J.* 25:4215–4222.